Mon. Not. R. Astron. Soc. **000**, 1–10 (♣) Printed 5 February 2008 (MN LATEX style file v2.2)

Spectral energy distribution of super-Eddington flows

D. Heinzeller[1,2⋆], S. Mineshige[2] and K. Ohsuga[3]
[1] *Zentrum für Astronomie Heidelberg, Institut für Theoretische Astrophysik, Albert-Ueberle-Straße 2, 69120 Heidelberg, Germany*
[2] *Yukawa Institute for Theoretical Physics, Kyoto University, Kitashirakawa-Oiwakecho, Sakyo-ku, Kyoto 606-8502, Japan*
[3] *Department of Physics, Rikkyo University, 3-34-1 Nishi-Ikebukuro, Toshimaku, Tokyo 171-8501, Japan*

Accepted ♣. Received ♣; in original form ♣

arXiv:astro-ph/0608263v1 12 Aug 2006

ABSTRACT

Spectral properties of super-Eddington accretion flows are investigated by means of a parallel line-of-sight calculation. The subjacent model, taken from two-dimensional radiation hydrodynamic simulations by Ohsuga et al. (2005), consists of a disc accretion region and an extended atmosphere with high velocity outflows. The non-gray radiative transfer equation is solved, including relativistic effects, by applying the flux limited diffusion approximation.

The calculated spectrum is composed of a thermal, blackbody-like emission from the disc which depends sensitively on the inclination angle, and of high energy X-ray and gamma-ray emission from the atmosphere. We find mild beaming effects in the thermal radiation for small inclination angles. If we compare the face-on case with the edge-on case, the average photon energy is larger by a factor of ~ 1.7 due mainly to Doppler boosting, while the photon number density is larger by a factor of ~ 3.7 due mainly to anisotropic matter distribution around the central black hole. This gives an explanation for the observed X-ray temperatures of ULXs which are too high to be explained in the framework of intermediate-mass black holes.

While the main features of the thermal spectral component are consistent with more detailed calculations of slim accretion discs, the atmosphere induces major changes in the high-energy part, which cannot be reproduced by existing models. We also conclude that, in order to interpret observational data properly, simple approaches like the Eddington-Barbier approximation cannot be applied.

Key words: super-Eddington accretion – spectral energy distribution – beaming

1 INTRODUCTION

With the constant improvement of observational techniques, more and more detailed information about accretion disc systems could be gained in the past decades. In particular, a large number of ultraluminous X-ray sources (ULXs) have been discovered since the end of the 1980's (Fabbiano 1989). These new astrophysical objects imposed a severe problem upon the existing general idea of accretion disc systems: With a bolometric luminosity exceeding $10^{39}\,\mathrm{erg\,s^{-1}}$ (derived from X-ray observations), at least some of them show relatively low radiation temperatures ($\sim 0.1\,\mathrm{keV}$). These systems have been suggested to be intermediate mass black hole (IMBH), sub-Eddington accretion disc systems (Miller et al. 2003; Cropper et al. 2004; Roberts et al. 2005). However, from stellar formation theory, it is difficult to explain the formation of IMBHs. Therefore, many different formation theories have been presented in the last years. A good overview can be found in van der Marel (2004) and Miller & Colbert (2004). Controversially, from time-variability observations, it seems to be likely that these objects are instead low-mass X-ray binary systems (Liu et al. 2002). Radio observations show that the distribution of ULXs can as well be fitted by stellar mass black holes with mildly relativistic jets (Körding et al. 2004).

With increasing observational data from X-ray satellites like ASCA, Chandra and XMM-Newton, large samples of ULX sources became available (e. g. Colbert & Mushotzky (1999); Makishima et al. (2000); Miller et al. (2004); Kubota & Makishima (2006)). They reveal that a distinct class of ULX sources exists, showing higher temperatures – sometimes exceeding 1 keV – than can be explained by IMBHs (e. g. Okada et al. (1998); Mizuno et al. (1999)). Contrary, stellar mass Kerr black holes accreting above their Eddington limit can account for these sources (Watarai et al. 2001; Ebisawa et al. 2003). Alternatively, mild beaming could be important (King et al. 2001), although the shape of the surrounding nebula indicates that it is illuminated by a nearly isotropic emission source

⋆ E-mail: dh@ita.uni-heidelberg.de

© ♣ RAS

(Wang 2002). A controversial debate about the origin of ULX sources is still ongoing.

Also in theory, a lot of investigations of accretion discs have been carried out in the past decades, not at last due to enhanced computational facilities. Systems hosting rotating black holes show higher temperatures and enhanced luminosities due to a smaller inner boundary, compared to their non-rotating counterparts (Gammie & Popham 1998; Popham & Gammie 1998). To bypass the violation of the Eddington limit for stellar mass black hole ULXs, various mechanisms have been proposed. Abramowicz et al. (1988) extended the standard thin disc model (Shakura & Sunyaev 1973) by considering advective energy transport, leading to so called "slim discs". These discs allow for higher mass accretion rates, compared to thin discs with the same luminosity. The photon bubble instability mechanism permits higher accretion rates and high luminosities while preserving the global stability of the disc (Begelman 2002). An important extension of the slim disc model is the full treatment of the photon trapping effects (see Katz (1977); Begelman (1978) for the case of spherical accretion): For sufficiently high accretion rates, the gas inflow time becomes shorter than the photon diffusion time in the inner part of the disc; high-energy photons otherwise emerging from the inner disc region are partially swallowed by the black hole, leading to altered spectral energy distributions and lower luminosities, compared to a standard slim disc (Ohsuga et al. 2002, 2003). The question about the validity of the Eddington limit in accretion discs itself is widely discussed, yielding strong deviations for these disc models (Heinzeller & Duschl 2006).

Also the emerging disc spectra have been investigated widely in the past: Simple blackbody or modified blackbody spectra for supercritical accretion discs have been calculated (Szuszkiewicz et al. 1996; Wang & Zhou 1999; Mineshige et al. 2000; Watarai et al. 2000). Furthermore, slim accretion disc spectra, including self-irradiation and self-occultation for self-similar solutions have been studied by Fukue (2000), while Watarai et al. (2005) investigated the implications of geometrical effects and general relativistic effects on the disc spectra. Further, Kawaguchi (2003) considered Comptonization effects in spectral calculations, finding significant spectral hardening occurring at large accretion rates. In these approaches, however, anisotropy in radiation fields is not taken into account, although we naively expect mild beaming effects, i. e., radiation is likely to escape predominantly in the direction perpendicular to the disc plane. Moreover, the influence of the environment of the disc, e. g. its atmosphere, is not considered. It is well known that accretion discs own extended atmospheres, which indeed have a strong influence on the emerging disc spectra. Photoionization of the accretion disc surface by incident X-rays has been investigated by Reynolds et al. (1999), while Dörrer et al. (1996) calculated disc spectra for a thin α-discs around a Kerr black hole, surrounded by a hydrogen atmosphere.

In this study, we calculate the spectral energy distribution of supercritical accretion flows based on the radiation hydrodynamic (RHD) simulations computed by Ohsuga et al. (2005). In Sect. 2, we describe the methods of calculations used in this investigation. Main aspects of the subjacent simulation data will also be briefly summarized there. We then present our spectral calculations in Sect. 3.

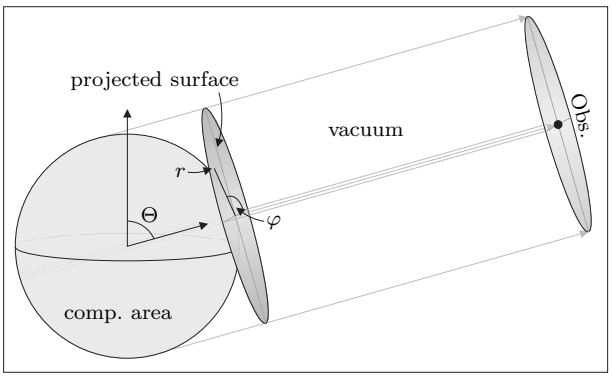

Figure 1. Sketch of the line-of-sight calculation

Discussion will be given in Sect. 4, while Sect. 5 is devoted to conclusions and an outlook.

2 MODEL SETUP

2.1 RHD simulations

In this study, we account for both a sophisticated disc model and the disc's atmosphere, computed in a self-consistent way within RHD simulations: we apply our calculations to the 2D RHD simulation data from Ohsuga et al. (2005). Starting with an empty disc and continuously injecting mass through the outer disc boundary, the authors simulated the structure of a supercritical accretion flow, until it reaches the quasi-steady state. The central object is given by a non-rotating stellar mass black hole ($M = 10 M_\odot$), generating a pseudo-Newtonian potential (Paczyński & Wiita 1980). The viscosity is given by the classical α prescription. The mass input rate at the outer boundary ($500 R_G$) strongly exceeds the Eddington limit, $\dot{M}_{\rm ext} = 1000 \dot{M}_E$, where $\dot{M}_E = L_E/c^2$. The authors considered energy transport through radiation and advection and included relativistic effects in the radiation part. Note that photon trapping effects were automatically incorporated in the simulations. A gray computation of the radiative transfer in the flux limited approximation (Levermore & Pomraning 1981) was used.

They found that the supercritical flow is composed of two parts: the disc region and the outflow regions above and below the disc. Within the disc region, the circular motion as well as the patchy density structure are observed. The mass accretion rate decreases inwards (i. e. as matter accretes), roughly in proportion to the radius, and the remaining part of the disc material leaves the disc to form an outflow. In particular, only 10% of the inflowing material finally reach the inner boundary ($3 R_G$), while the remaining 90% get stuck in the dense, disc-like structure around the midplane or transform into moderately high-velocity outflows with wide opening angles. The outflows are accelerated up to $\sim 0.1c$ via strong radiation pressure force.

From the simulation data, the gas density ρ, its temperature $T_{\rm gas}$ and its velocity v are taken as input parameters, as well as the radiation energy density E. The methods of calculating other quantities, such as the radiation temperature $T_{\rm rad}$, the source function S_ν and the radiation pressure tensor P_ν, will be given in the following subsections.

2.2 Equation of radiative transfer

Under the assumption of an observer being located at infinite distance from the object, we calculate the emerging flux/luminosity as a function of the observers inclination angle Θ and azimuthal angle Φ. Here, Θ and Φ refer to the spherical coordinate system which describes the computational box.[1]

More precisely, we adopt a parallel line-of-sight calculation on a two-dimensional grid on the projected surface, seen by the observer (see Fig. 1 for a better understanding). We start the line-of-sight calculation at a sufficiently high optical depth $\tau_{\nu,\mathrm{start}}$ from the projected surface with initial intensity $I_\nu = 0$ and with fixed direction cosine vector $\vec{l} = \vec{l}(\Theta, \Phi)$.

We focus on solving the radiative transfer equation numerically by a Runge-Kutta algorithm, considering the relativistic corrections due to the high velocities of the gas. General relativistic effects such as gravitational lensing and gravitational redshift are not taken into account. We have to distinguish between two different coordinate systems: We describe the system in which the observer and the computational area are in rest with I_ν, l, etc., while the same quantities are tagged with 0 in the frame comoving with the local gas velocity $\vec{v}$. Since the gas velocity strongly varies, the comoving frame depends on the position in the simulation box.

In this framework, the relativistic equation of radiative transfer is given by

$$(\vec{l}\cdot\vec{\nabla})I_\nu = \left(\frac{\nu}{\nu_0}\right)^2 \cdot \left\{ \kappa^{\mathrm{abs}}_{\nu_0} S_{\nu_0} - \chi_{\nu_0} I_{\nu_0} + \frac{3}{4}\kappa^{\mathrm{sca}}_{\nu_0} \frac{c}{4\pi}\left(E_{\nu_0} + l_{0i} l_{0j} P^{ij}_{\nu_0}\right) \right\}, \quad (1)$$

while, in the non-relativistic case, it reduces to

$$(\vec{l}\cdot\vec{\nabla})I_\nu = \left\{ \kappa^{\mathrm{abs}}_{\nu} S_{\nu} - \chi_{\nu} I_{\nu} + \frac{3}{4}\kappa^{\mathrm{sca}}_{\nu} \frac{c}{4\pi}\left(E_{\nu} + l_i l_j P^{ij}_{\nu}\right) \right\}. \quad (2)$$

It is important to note that all quantities on the right hand side of (1) are evaluated in the comoving frame, while those on the left hand side are given in the rest frame. In the equation of radiative transfer, S_ν denotes the source function for matter, E_ν the radiation energy density and $\mathbf{P}_\nu$ the radiation pressure tensor. Additionally, $\chi_\nu = \kappa^{\mathrm{abs}}_\nu + \kappa^{\mathrm{sca}}_\nu$.

In this first approach, we restrict ourself to frequency-dependent absorption coefficients for free-free absorption processes and totally neglect bound-free absorption processes, $\kappa^{\mathrm{abs}}_\nu = \kappa^{\mathrm{ff}}_\nu$. This holds as a good approximation, since the gas temperature is mostly above 10^5 K, and, hence, hydrogen is fully ionized. For simplicity, we do not consider for metal opacities. We adopt the formula given in Rybick & Lightman (1979),

$$\kappa^{\mathrm{ff}}_\nu = 3.7 \cdot 10^8 T^{-1/2}\left(\frac{\rho}{m_p}\right)^2 \nu^{-3}\left(1 - e^{-h\nu/kT}\right)\ \mathrm{cm}^{-1}, \quad (3)$$

[1] Note that the equatorial plane of the computational box is defined by the injection point of gas and its angular momentum vector.

where we assume the mass density of ions and electrons to be equal, $\rho = \rho_i = \rho_e$. For the scattering processes, we only consider electron scattering, given by

$$\kappa^{\mathrm{sca}} = \sigma_T\left(\frac{\rho}{m_p}\right)\mathrm{cm}^{-1}. \quad (4)$$

The relativistic transformation rules are

$$\nu_0 = \nu\Gamma\left(1 - \frac{\vec{v}\cdot\vec{l}}{c}\right) \quad (5)$$

$$\vec{l}_0 = \frac{\nu}{\nu_0}\left[\vec{l} + \left(c\frac{\Gamma - 1}{\vec{v}^2}\vec{v}\cdot\vec{l} - \Gamma\right)\frac{\vec{v}}{c}\right] \quad (6)$$

$$I_{\nu_0} = \left(\frac{\nu_0}{\nu}\right)^3 I_\nu \quad (7)$$

with Γ being the Lorentz factor.

2.3 Frequency-dependent radiation quantities

Special attention is needed for deriving the quantities S_ν and E_ν (and therefore, by applying the flux limited diffusion approximation – see Sect. 2.4 – also $\mathbf{P}_\nu$). As the radiative transfer in the 2D RHD simulation is calculated in a gray approximation, the simulation data provides only frequency-integrated values for the radiation energy density. The matter distribution is described by the gas density and gas temperature. We assume local thermal equilibrium for the matter distribution and for the radiation field separately:

$$S_{\nu_0} = B_{\nu_0}(T_{\mathrm{gas}}) = \frac{2h\nu_0^3}{c^2}\cdot\frac{1}{\exp\left(\frac{h\nu_0}{k_B T_{\mathrm{gas}}}\right) - 1} \quad (8)$$

$$T_{\mathrm{rad}} = \left(\frac{E}{a}\right)^{1/4}, \quad a = \text{ radiation constant} \quad (9)$$

$$E_{\nu_0} = \frac{4\pi}{c} B_{\nu_0}(T_{\mathrm{rad}}) \quad (10)$$

While (8) generally holds as a good approximation, (9) and (10) have to be treated carefully: In a scattering dominated domain as it is the case in the underlying simulation data here, photons undergo multiple scattering and therefore expand in space – accordingly, the radiation field is diluted and the photon number decreases. This implies that the average photon temperature will be underestimated by (9) and (10), which will be discussed later (Sect. 4). Therefore, we henceforth focus our discussion on the relative changes of the flux, photon energy and photon number due to the variations of the inclination angle Θ.

2.4 Flux limited diffusion approximation

To calculate the radiation pressure tensor, we apply the frequency-dependent flux limited diffusion (FLD) approximation (Levermore & Pomraning 1981) to the quantities in the comoving frame. In this context, the radiation pressure tensor can be expressed by

$$\mathbf{P}_{\nu,0} = \mathbf{f}_\nu E_{\nu,0}, \quad (11)$$

where $\mathbf{f}_\nu$ is called the Eddington-tensor. Its components are given by

$$f^{ij}_\nu = \frac{1}{2}(1 - f_\nu)\delta^{ij} + \frac{1}{2}(3f_\nu - 1)n^i_\nu n^j_\nu. \quad (12)$$

Here, n^i denotes the normalized energy density gradient,

$$n_\nu^i = \frac{\left(\vec{\nabla} E_\nu\right)^i}{\left|\vec{\nabla} E_\nu\right|} \,. \tag{13}$$

Following Kley (1989), n_ν^i and subsequent quantities can be expressed as functions of the energy density in the inertial frame.

To close the resulting equations, the Eddington factor f_ν has to be determined. From the momentum equations, the relation between f_ν and λ_ν is given by

$$f_\nu = \lambda_\nu + \lambda_\nu^2 \mathcal{R}_\nu^2 \,, \qquad \mathcal{R}_\nu = \frac{\left|\vec{\nabla} E_\nu\right|}{\chi_\nu E_\nu} \,. \tag{14}$$

The flux limiter λ_ν itself can not be determined from the equations of radiative transfer, but has to be defined manually. In order to do so, two conditions have to be fulfilled. In the case of $\chi_\nu \to \infty$, the equations have to reduce to the classical diffusion limit, i. e. $\lambda_\nu \to \frac{1}{3}$. In the case of $\chi_\nu \to 0$, the flux limiter must tend towards $1/\mathcal{R}_\nu$ in order to ensure $|\vec{F}_{\nu,0}| \leqslant c E_{\nu,0}$.

Naturally, there exist multiple possibilities to describe the flux limiter λ_ν. We adopt the common formulation from Levermore & Pomraning (1981):

$$\lambda_\nu(\mathcal{R}_\nu) = \frac{2 + \mathcal{R}_\nu}{6 + 3\mathcal{R}_\nu + \mathcal{R}_\nu^2} \tag{15}$$

2.5 Numerics

In the present investigation we choose a *single* snapshot of the RHD simulation data after the simulation settled down in a quasi-steady structure. In this stadium, the structure does not change anymore in time in a significant way, giving rise to consider our results as characteristic properties of such a system.[2]

The calculation of the disc spectra is performed as presented above with and without relativistic corrections. As the simulation data is symmetric with respect to the azimuthal angle Φ, we compute the spectra only in dependency of the inclination angle Θ. We investigate the results of the computation for different starting points (i. e., optical depths $\tau_{\nu,\mathrm{start}}$) for the line-of-sight calculation. For $\tau_{\nu,\mathrm{start}} \approx 8$, the results begin to saturate, leading to changes below 1% when starting at higher optical depths. We used $\tau_{\nu,\mathrm{start}} = 10$ throughout all cases and validated the results with several integrations from $\tau_{\nu,\mathrm{start}} = 10$, yielding differences below 10^{-3}.

The reason why such a low $\tau_{\nu,\mathrm{start}}$ reveals the same results than higher optical depths can be understood from the two extreme cases:

(i) the gas is dense and cool with $T_{\mathrm{gas}} \approx T_{\mathrm{rad}}$ and small contributions of the gas to the total emissivity
(ii) it is diluted such that $\kappa_\nu^{\mathrm{abs}} \ll \kappa_\nu^{\mathrm{sca}}$ and the total emission along the line of sight is completely dominated by the radiation field

For all calculations it turns out that increasing gas temperatures go hand in hand with dropping gas densities so that the opacity and total emission are governed by the radiation field.

[2] For details, we refer the reader to Ohsuga et al. (2005).

We divide the projected surface seen by the observer in a polar grid with coordinates (r, φ), see Fig. 1. Both for the radial and the polar coordinate, we adopt a linear grid with $N_r = 100$ and $N_\varphi = 200$ grid points. The discretization in frequency is taken to be logarithmic with $N_\nu = 200$ frequency values between 10^{14} Hz (0.5 eV) and 10^{22} Hz (50 MeV).

3 RESULTS

3.1 Overall spectral properties

Figure 2 shows the resulting spectrum νL_ν for inclination angles $\Theta = 0, \pi/4$ and $\pi/2$ with and without relativistic corrections. The luminosity is given by

$$L_\nu(\Theta) = 4\pi \int_A I_\nu(\Theta, r, \varphi)\, dA \,, \tag{16}$$

where A denotes the projected surface of the computational area, as it is seen by the observer. For low frequencies, the spectra only weakly depend on the viewing angle. Also, relativistic corrections are unimportant for energies $\lessapprox 400$ eV ($\nu \lessapprox 10^{17}$ Hz). Contrary, for higher energies, the dependency on the viewing angle becomes stronger. For high inclinations, i. e. for an edge-on view on the system, relativistic corrections still remain unimportant, while they become drastically visible for low inclinations, i. e. for a nearly face-on view on the disc. For both the relativistic and the non-relativistic case, an enhancement of the peak frequency and luminosity is observable for small inclination angles; although, this boost is much stronger when considering relativistic corrections. Furthermore, instead of a rapid drop of νL_ν for high energies, a slower decline up to a plateau-like structure can be seen in all cases.

Figure 3 illustrates again the spectrum for $\Theta = 0$. To show that the observed plateau in Figs. 2 and 3 is a result of the thermal emission $\kappa^{\mathrm{abs}} S_\nu$ from the hot gas in the photosphere, we calculate the spectrum without gas contribution, i. e. we set $S_{\nu,\mathrm{gas}} = 0$ everywhere. As it can be seen from the figure, the high-energy plateau disappears completely when neglecting the contribution from the hot gas, confirming our hypothesis. We want to remark that

(i) this structure may by altered significantly if Compton scattering is taken into account, since this provides an effective cooling mechanism for the gas. However, the inclusion of Compton scattering and the calculation of the decrease in T_{rad} is beyond the scope of this work.
(ii) it is unlikely to observe this plateau since the overall emission in this energy range is considerably low and the spectrum is dominated by the peak emission.

To illustrate the influence of the disc's environment in the face-on case in Fig. 3, we calculate the spectrum for a "screened" central region (for $R \leqslant 100 R_G$, we set all physical quantities to zero) and for the core region only (for $R \geqslant 100 R_G$, all physical quantities are set to zero). Here, R denotes the radial coordinate in the spherical coordinate system describing the computational box. The former case corresponds to a system where the inner $100 R_G$ are entirely evacuated and so emission, absorption and scattering processes only exist outside the core region. Contrarily, the latter case means that no emission, no absorption and no scat-

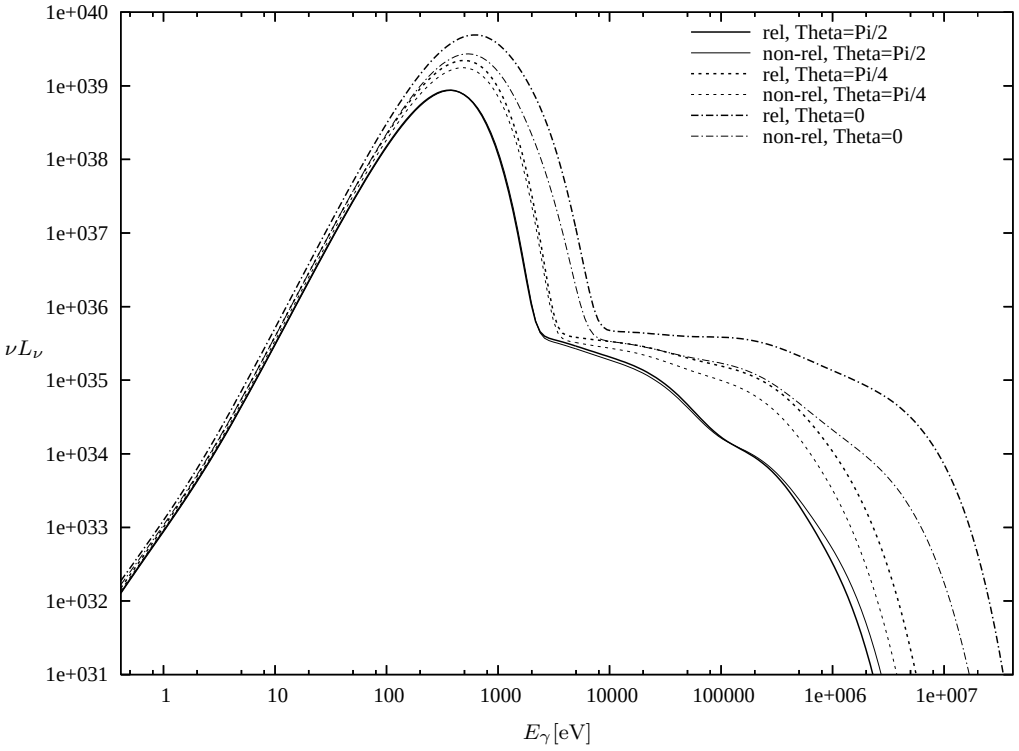

Figure 2. Disc spectra νL_ν for inclination angles $\Theta = 0, \pi/4, \pi/2$ with and without relativistic corrections

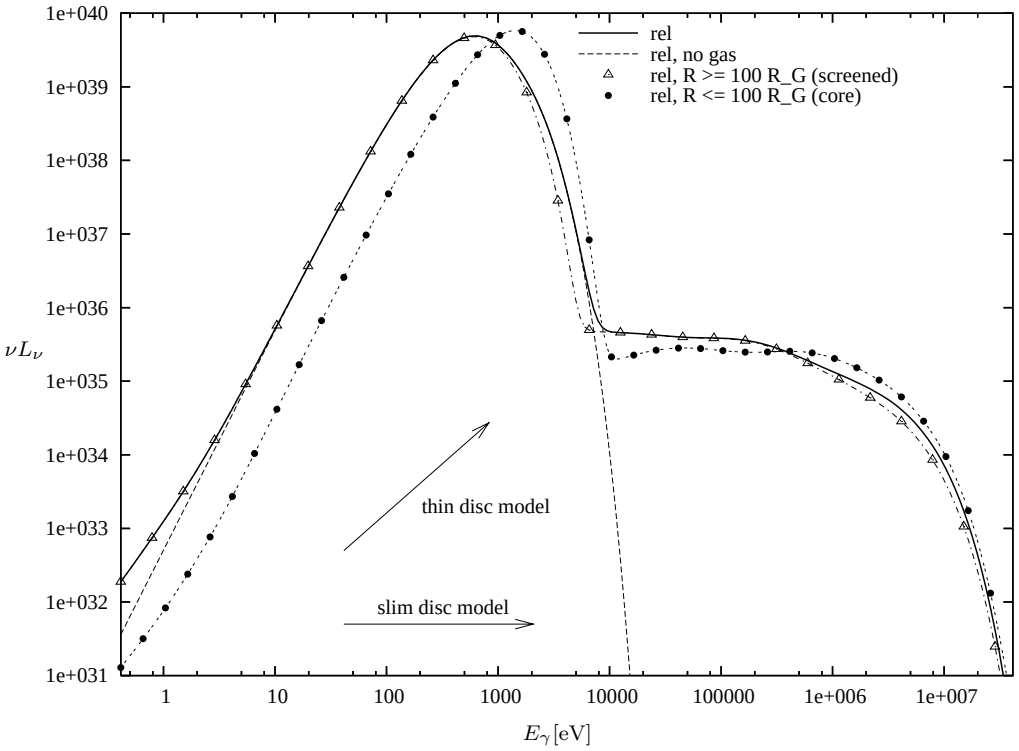

Figure 3. Disc spectra νL_ν for $\Theta = 0$ with relativistic corrections. Beneath the normal spectrum (as in Fig. 2), we plot the spectra without gas contributions, for the core region only ($R \leqslant 100 R_G$) and for a screened inner region ($R \geqslant 100 R_G$). Additionally, theoretical spectral shapes for thin and slim accretion discs are sketched

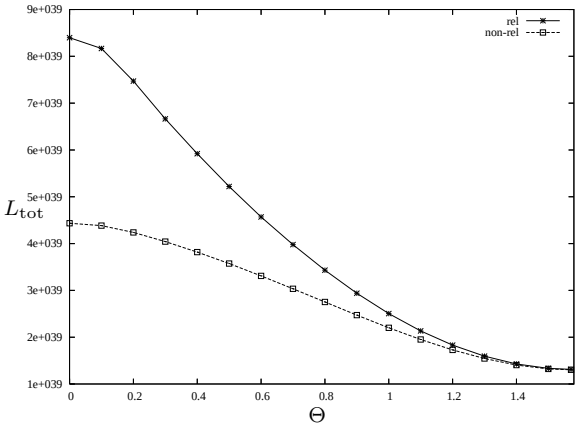

Figure 4. Total luminosity $L_{\rm tot}$ as a function of the viewing angle Θ for the relativistic and non-relativistic calculation

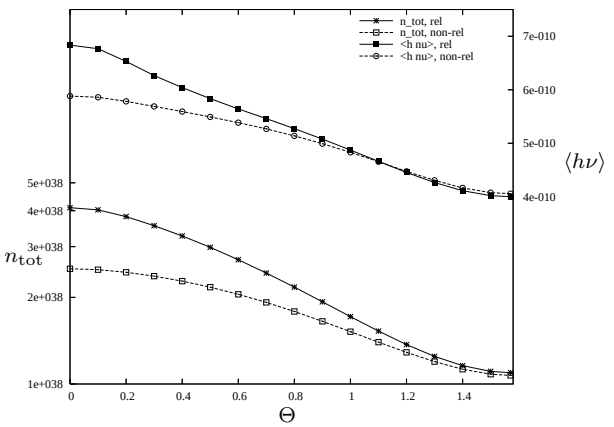

Figure 5. Total photon number density $n_{\rm tot}$ and average photon energy $\langle h\nu \rangle$ in the relativistic and non-relativistic case as functions of the inclination angle Θ (see text for details)

tering takes place for $R \geqslant 100 R_G$, yielding the unaltered emission from the core region only. Obviously, the environment of the disc has a rather strong influence on the emerging spectrum.

Furthermore, the theoretical spectral shapes for a standard thin α-disc (Shakura & Sunyaev 1973) and for a standard slim disc (Abramowicz et al. 1988) are indicated in Fig. 3, each time without consideration for self-irradiation, atmosphere, relativistic effects, etc. By just taking into account the surface temperature $T_{\rm eff}$ for these disc models and taking advantage of the face-on view (no self-occultation), $\nu L_\nu \propto \nu^{4/3}$ for the thin disc case, and $\nu L_\nu \propto \nu^0$ for the slim disc case (see, e. g., Kato et al. (1998, Sect. 3.2.5)). These shapes do not coincide with our results, although they should be valid at least for the peak intensity region of the spectrum.

3.2 Angular dependence of the luminosity

In Fig. 4, we show the dependency of the total luminosity

$$L_{\rm tot}(\Theta) = \int L_\nu(\Theta)\, d\nu \qquad (17)$$

on the viewing angle for both the relativistic and the non-relativistic calculation. The energy boost for small inclination angles appears in both cases, although it is stronger for the relativistic calculation. Due to relativistic effects, the gain in luminosity compared to the non-relativistic calculation $L_{\rm tot}^{\rm rel}/L_{\rm tot}^{\rm non\text{-}rel}$ varies between 1.0 for $\Theta = \pi/2$ and 1.9 for $\Theta = 0$.

We thus conclude that $L_{\rm tot}$ is by a factor of ~ 6.4, at most, enhanced for a face-on observer, compared with an edge-on observer. The increase in total luminosity may be due either to an increase in photon number or an increase in average photon energy. Which one is more important?

To answer this question and to outline the relativistic effects more explicitly, we plot in Fig. 5 the total photon number density $n_{\rm tot}$ and the average photon energy $\langle h\nu \rangle$ as a function of the inclination angle. From our SEDs, we calculate the photon number density by

$$n_{\rm tot}(\Theta) = \int n_\nu(\Theta)\, d\nu = \int \frac{L_\nu(\Theta)}{h\nu c}\, d\nu \qquad (18)$$

and from that, the average photon energy by $\langle h\nu \rangle(\Theta) = L_{\rm tot}(\Theta)/(c n_{\rm tot}(\Theta))$. While relativistic effects become more or less unimportant in the the edge-on case, they cause an additional increase both in total number of photons originating from the system and in average photon energy in the face-on case. Table 1 summarizes the gain in total luminosity, photon number and average photon energy for the face-on case – this means, the ratio for each of the quantities for $\Theta = 0$, compared to inclination angles between 0 and $\pi/2$.

Table 1. Gain in total luminosity, photon number and average photon energy for the face-on case (see text for details)

Θ	$L_{\rm tot}$		$n_{\rm tot}$		$\langle h\nu \rangle$	
	rel.	non-rel.	rel.	non-rel.	rel.	non-rel.
0	1.00	1.00	1.00	1.00	1.00	1.00
$\pi/6$	1.66	1.26	1.41	1.17	1.18	1.08
$\pi/4$	2.40	1.59	1.86	1.39	1.29	1.14
$\pi/3$	3.63	2.14	2.53	1.72	1.43	1.24
$\pi/2$	6.40	3.40	3.74	2.35	1.71	1.45

The results given in Table 1 can be explained physically as follows: Starting from the *non-relativistic* calculation, we find that

- lower densities and therefore less effective absorption and scattering in the photosphere allow a deeper look into the hotter region for the face-on case, compared to the edge-on case. Hence, the average photon energy $\langle h\nu \rangle$ is increased by a factor of 1.45.
- photons can escape more easily through the diluted medium along the polar axis, while they get stuck in the dense disc-like structure concentrated in the midplane. The outflow is therefore collimated and the number of escaping photons raised by a factor of 2.35.

At the same time, the (outflow) velocities of the gas close to the black hole ($R \lessapprox 100 R_G$) and around the polar axis are higher, which becomes important for the *relativistic* calculation.

- The frequency of the escaping photons is shifted from ν to $\nu_0 \geqslant \nu$ by the relativistic Doppler effect, increasing the average photon energy additionally by a factor of

$1.71/1.45 = 1.18$, when comparing the face-on with the edge-on view.

- Since the relativistic invariant is I/ν^3, the emerging intensity in the relativistic calculation, compared to the non-relativistic case is given by $I_0/I \sim (\nu_0/\nu)^3$. One factor of ν_0/ν directly goes into $\langle h\nu \rangle$ via the relativistic Doppler effect, the remaining factor of $(\nu_0/\nu)^2$ applies to the emerging photon number $n_\nu \sim I_\nu/(h\nu)$, raising it once more by factor of $3.74/2.35 = 1.59$, when Θ decreases from $\pi/2$ to 0.

All in all, an observer located at $\Theta = \pi/2$ only sees the emission from the outer part of the optically thick disc-like structure, which itself screens the relativistic effects in the inner region of the system. The radial velocities and also the azimuthal velocities are relatively low ($v_\varphi \approx 0.01c$). For the mainly contributing part to the spectrum, the azimuthal velocity is (almost) perpendicular to the line of sight, therefore the already weak relativistic effects are not detectable for an edge-on observer. In the face-on case, the highly relativistic flow ($v_\mathrm{s} \lessapprox 0.3c$) can by observed due to the optically thin atmosphere above the disc. At the same time, the radial velocity is pointing into the direction of the observer, leading to strong enhancements of the radiative flux at low inclinations.

3.3 Blackbody fitting

When spectral data of binary black hole sources are obtained, it is usual to fit them with blackbody (or disc blackbody) spectra. We thus attempt a similar spectral fitting to our theoretically calculated spectra: We apply a non-linear least square fit to the emerging intensity I_ν by a blackbody spectrum with temperature T_fit, altered by a spectral hardening factor ε (Soria & Puchnarewicz 2002). The fitting function is then given by

$$f = f(\nu, \varepsilon, T_\mathrm{fit}) = \varepsilon^{-4} \cdot \frac{2h\nu^3}{c^2} \cdot \frac{1}{\exp\left(\frac{h\nu}{\varepsilon k_B T_\mathrm{fit}}\right) - 1}\,. \qquad (19)$$

Note that the factor ε^{-4} is introduced to ensure the same radiation energy loss:

$$\pi \cdot \int f(\nu, \varepsilon, T_\mathrm{fit})\, d\nu = \varepsilon^{-4} \sigma (\varepsilon T_\mathrm{fit})^4 = \sigma T_\mathrm{fit}^4 \qquad (20)$$

In order to account for stochastic fluctuations, we weigh the fitting coefficients by their relative intensity. So, the weight-function is given by

$$w(\nu) = \frac{I_\nu}{I_\mathrm{tot}}, \qquad I_\mathrm{tot} = \int I_\nu\, d\nu\,. \qquad (21)$$

Figure 6 shows the results for the fitting temperatures T_fit as a function of the inclination angle Θ. Additionally, we plot the surface-averaged radiation temperatures

$$\bar{T}_\mathrm{rad} = \frac{1}{A} \int_A T_\mathrm{rad}\, dA \qquad (22)$$

at optical depths $\tau_\nu = 1$ and $\tau_\nu = 10$. As mentioned earlier, the temperature of the radiation field will be underestimated by (9) and (10). We therefore concentrate on its relative changes for different inclinations and scale all temperatures to the fitting temperature T_fit at $\Theta = \pi/2$, where it is basically the same for the relativistic and for the non-relativistic calculation.

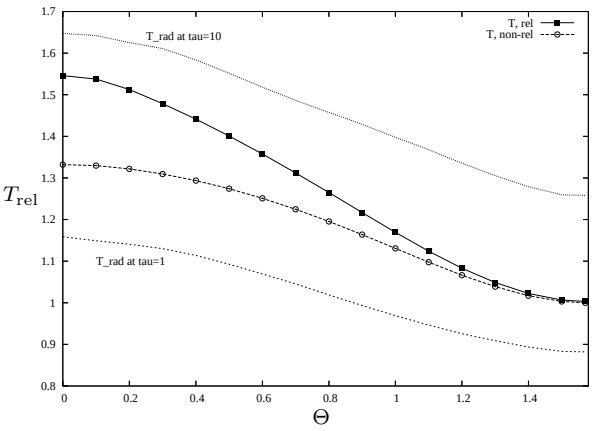

Figure 6. Fitted blackbody temperatures for the relativistic and non-relativistic calculation as a function of the viewing angle Θ. Additionally, mean temperatures at $\tau_\nu = 1$ and $\tau_\nu = 10$ are shown. All temperatures are scaled by T_fit at $\Theta = \pi/2$

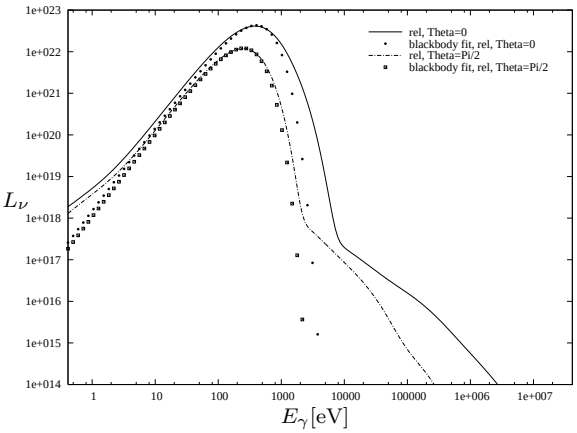

Figure 7. Luminosity L_ν and the corresponding blackbody fits for the face-on and edge-on case

If neglecting relativistic corrections, the fitted blackbody temperature is given roughly by the radiation temperature at a *constant* optical depth between 1 and 10. The blackbody temperature rises by a factor 1.3 when switching from an edge-on to a face-on case. The spectrum is only weakly hardened compared to a Planck distribution at the same temperature T_fit: The spectral hardening factor ε adopts an almost constant value close to unity, $\varepsilon \approx 1.15$, for all inclinations.

When accounting for relativistic corrections, no surface of constant optical depth can be defined any more: While the fitting temperatures resemble those of the non-relativistic case for high inclinations, they differ significantly for low inclinations, mirroring the above statement of stronger relativistic effects for the face-on seen system. While the blackbody temperature rises by a factor of 1.6, the hardening factor ε stays almost constant around 1.15, like in the non-relativistic calculation.

Finally, Fig. 7 shows the luminosity L_ν for the face-on and edge-on view and the corresponding blackbody fits in the relativistic case. Due to the weighting function, the peak intensity region is fitted quite well, while there are large deviations in the low-energy and high-energy part.

4 DISCUSSION

The results presented in Sect. 3 permit to draw several conclusions about the observational appearance of supercritical accretion disc systems.

It is clearly not sufficient to consider only the disc and neglect its surroundings like its hot photosphere, outflow regions, etc. Their influence becomes most important in the high-energetic part of the spectrum ($h\nu \gtrapprox 4\,\mathrm{keV}$). We find a plateau-like structure, independent of relativistic effects and of the viewing angle, which can be ascribed directly to the high gas temperature in the corona. Therefore, neither the basic thin disc spectrum, nor the basic slim disc spectrum fit to our results.

Our results also confirm that the Eddington-Barbier approximation, a common simplification of radiative transfer calculations for stellar atmospheres, cannot be applied in accretion discs: In this approximation, one generally assumes that the emergent intensity along the line of sight is equal to the source function at constant optical depth $\tau = 2/3$. In our calculation, the main contribution to the emerging flux is produced at higher optical depths $\tau_{\mathrm{eff}} > 2/3$; moreover, the exact value of τ_{eff} depends on the inclination angle.

We observe an enhanced luminosity for more and more face-on seen systems, which is due to both enhanced average photon energy and total photon number. Relativistic effects alter the total photon number much more significantly (almost twice the non-relativistic treatment) than the average photon energy. This can be identified as *mild relativistic beaming*.

As mentioned above, due to (9) and (10), the resulting fit temperatures underestimate the real temperature of the radiation field. Strictly speaking, the temperature of the radiation field should be determined at $\tau^* \approx 1$ ($\tau^* \sim \sqrt{\tau^{\mathrm{sca}}\tau^{\mathrm{abs}}}$) and not at $\tau \approx 1$ (in a scattering dominated domain, $\tau \sim \tau^{\mathrm{sca}}$). Hence, the radiation energy density E_ν will resemble more a shifted black body distribution with a colour-corrected temperature T_{col},

$$E_\nu \sim B_\nu(T_{\mathrm{col}})\sqrt{\kappa_\nu^{\mathrm{abs}}/\kappa^{\mathrm{sca}}}\,, \tag{23}$$

rather then (10), where $E_\nu \sim B_\nu(T_{\mathrm{fit}})$. From the requirement of energy conservation,

$$E = \int B_\nu(T_{\mathrm{fit}})\,d\nu = \int B_\nu(T_{\mathrm{col}})\sqrt{\frac{\kappa_\nu^{\mathrm{abs}}}{\kappa^{\mathrm{sca}}}}\,d\nu\,. \tag{24}$$

To get a rough idea on how much the derived temperatures are underestimated, we solve (24) numerically for T_{col} in the main emanating region of radiation ($\tau \approx 10$). This yields a correction factor $\xi = T_{\mathrm{col}}/T_{\mathrm{fit}} \approx 10$. With

$$T_{\mathrm{fit}} = \left[9.4\cdot 10^5\mathrm{K}\ldots 1.4\cdot 10^6\mathrm{K}\right] \tag{25}$$

for $\Theta = [\pi/2\ldots 0]$, this leads to colour-corrected temperatures in the range of

$$T_{\mathrm{col}} = \left[9.4\cdot 10^6\mathrm{K}\ldots 1.4\cdot 10^7\mathrm{K}\right] \tag{26}$$

These temperatures would be consistent with the observed high temperatures of several ULX sources (Makishima et al. 2000) that can not be explained in terms of intermediate mass black hole systems with sub-Eddington accretion rates. However, our approach is certainly too simplified to answer this "too hot accretion disc" puzzle in a satisfactory way.

In this work, spectral hardening turns out to be negligible. This may be due in parts to the assumption of Thomson scattering: Comptonization effects are expected to harden the spectrum significantly (Czerny & Elvis 1987; Ross, Fabian & Mineshige 1992; Kawaguchi 2003). Then, if only the peak of the spectrum is observed, the absolute scale and therefore the spectral hardening factor ε remains unknown and the observed temperature $T_{\mathrm{obs}} = \varepsilon T_{\mathrm{col}}$ overestimates the colour temperature T_{col}. Moreover, bulk motion Compton scattering is known to alter photon energies due to the angular redistribution of the scattered photons (Psaltis & Lamb 1997). Socrates, Davis & Blaes (2004) showed that turbulent Comptonization produces a significant contribution to the far-UV and X-ray emission of black hole accretion discs.

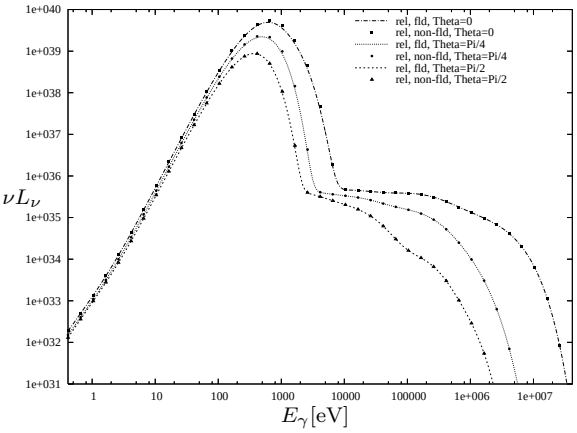

Figure 8. Disc spectra νL_ν for $\Theta = 0, \pi/4, \pi/2$, computed under the FLD approximation and complete isotropy

A weak point in our investigation is the application of the flux limited diffusion approximation instead of solving the full momentum equations: In this approximation, several terms in the equation of radiative transfer (1), like $1/c^2\,(DF/Dt)$ with F being the absolute value of the flux, are dropped. These terms are of the order of v/c and may contribute to the relativistic effects we find in our spectral calculations. By calculating the emerging spectra under the classical diffusion limit (i. e. complete isotropy, $\lambda = 1/3$), we find only little influence of the FLD approximation at all (see Fig. 8). Thus, the inconsistencies invoked by applying the flux limited diffusion approximation do not affect our results in a significant way.

5 CONCLUSION AND OUTLOOK

Our radiative transfer calculations, based on the 2D RHD simulation of highly accreting supercritical discs including the photon trapping mechanism, show that the interpretation of observed disc spectra is not a straightforward task. Especially, we find moderate beaming effects when the system is viewed from nearly face-on; i. e., the average photon energy is larger by a factor of ~ 1.7 in the face-on case than in the edge-on case due mainly to the Doppler boosting. Likewise, the photon number density is larger by a factor of ~ 3.7 because of the anisotropic matter distribution around the central black hole. Interpreting observations thus has to be done in a more sophisticated way than one may expect from basic disc models: It requires a careful treatment of the

radiative transfer with consideration for the discs surroundings.

We assume that both the gas and the radiation field separately stay in local thermal equilibrium. Although the weak coupling of matter and radiation ($\kappa_{\rm abs} \ll \kappa_{\rm sca}$) supports this assumption, it remains questionable and also underestimates the temperature of the radiation field. It is important to note that previous investigations by Wang et al. (1999); Fukue (2000); Watarai et al. (2005) also rely on this approximation; nevertheless, their results differ in a significant way. Solving the crux of assuming LTE for the gas and for the matter distribution at the present stage is not possible, because it requires frequency-dependent RHD simulations.

In a next step, Compton scattering has to be included as well as frequency-dependent absorption for both continuum (bound-free absorption may become relevant in the low-energetic tail of the SED) and line processes: From the observational side, emission lines, especially the K-shell transitions of iron, are a prominent feature in accretion disc system and comprise many details about the observed object (see Reynolds et al. (1999); Reynolds (2006) for example). Beneath the effects on the high-energetic part of the spectrum mentioned before, Compton scattering will provide an efficient cooling mechanism for the hot gas.

As pointed out by Watarai et al. (2005), also general relativistic effects should be considered in the vicinity of the black hole, which will primarily affect the spectra of face-on seen systems.

ACKNOWLEDGMENTS

The authors would like to thank Dr. Ken-ya Watarai, and Profs. Wolfgang J. Duschl, Jun Fukue and Shoji Kato for useful comments and discussions. This work was supported in part by the Grants-in-Aid of the Ministry of Education, Science, Culture, and Sport (14079205, 16340057 S.M.), by the Grant-in-Aid for the 21st Century COE "Center for Diversity and Universality in Physics" from the Ministry of Education, Culture, Sports, Science and Technology (MEXT) of Japan, and by the International Max Planck Research School for Astronomy and Cosmic Physics at the University of Heidelberg.

REFERENCES

Abramowicz M.A., Czerny B., Lasota J.P., Szuzkiewicz E., 1988, ApJ, 332, 646
Begelman M.C., 1978, MNRAS, 184, 53
Begelman M.C., 2002, ApJ, 568, L97
Colbert E.J.M., Mushotzky R.F., 1999, ApJ, 519, 89
Cropper M., Soria R., Mushotzky R.F., Wu K., Markwardt C.B., Pakull M., 2004, MNRAS, 349, 39
Czerny B., Elvis M., 1987, ApJ, 321, 305
Dörrer T., Riffert H., Staubert R., Ruder H., 1996, A&A, 311, 69
Fabbiano G., 1989, ARA&A, 27, 87
Fukue J., 2000, PASJ, 52, 829
Ebisawa K., Zycki P., Kubota A., Mizuno T., Watarai K.-y., 2003, CHJAA, 3, Suppl., 415
Gammie C.F., Popham R., ApJ 498 (1998), 313–326
Hayashi C., Hoshi R., Sugimoto D., 1962, Progr. Theoret. Phys. Supp., 22, 1
Heinzeller D., Duschl W.J., 2006, to appear
Kato S., Fukue J., Mineshige S., 1998, Black-Hole Accretion Disks. Kyoto University Press, Kyoto
Katz J.I., 1977, ApJ, 215, 265
Kawaguchi T., 2003, ApJ, 593, 69
King A.R., Davies M.B., Ward M.J., Fabbiano G., Elvis M., 2001, ApJ, 552, L109
Kley W., 1989, A&A, 208, 98
Körding E., Colbert E., Falcke H., 2004, Progr. Theoret. Phys. Supp., 155, 365
Kubota A., Makishima K., 2004, Advances in Space Research, Proc. of 35th COSPAR, Paris, France, in press
Levermore C.D., Pomraning G.C., 1981, ApJ, 248, 321
Liu J.-F., Bregman, J.N., Irwin J., Seitzer P., 2002, ApJ, 581, L93
Makishima K. et al., 2000, ApJ, 535, 632
van der Marel R.P., 2004, Intermediate-Mass Black Holes in the Universe: A Review of Formation Theories and Observational Constraints. Carnegie Observatories Centennial Symposia, Coevolution of Black Holes and Galaxies. Cambridge University Press, Cambridge
Miller J.M., Fabbiano G., Miller, M.C., Fabian A.C., 2003, ApJ, 585, L37
Miller J.M., Zezas A., Fabbiano G., Schweizer F., 2004, ApJ, 609, 728
Miller M.C., Colbert E.J.M., 2004, Int. J. Mod. Phys. D, 13, 1
Mineshige S., Kawaguchi T., Takeuchi M., Hayashida K., 2000, PASJ, 52, 499
Mizuno T., Ohnishi T., Kubota A., Makishima K., Tashiro M., 1999, PASJ, 51, 663
Ohsuga K., Mineshige S., Mori M., Umemura M., 2002, ApJ, 574, 315
Ohsuga K., Mineshige S., Mori M., Watarai K.-y., 2003, ApJ, 596, 429
Ohsuga K., Mori M., Nakamoto T., Mineshige S., 2005, ApJ, 628, 368
Okada K., Dotani T., Makishima K., Mitsuda K., Mihara T., 1998, PASJ, 50, 25
Paczyński B., Wiita P.J., 1980, A&A, 88, 23
Popham R., Gammie C.F., 1998, ApJ, 504, 419
Psaltis D., Lamb F.K., 1997, ApJ, 488, 881
Reynolds C.S., 2006, preprint (astro-ph/0605368)

Reynolds C.S., Young A.J., Begelman M.C., Fabian A.C., 1999, ApJ, 514, 164
Roberts T.P., Warwick R.S., Ward M.J., Goad M.R., Jenkins L.P., 2005, MNRAS, 357, 1363
Ross R.R., Fabian A.C., Mineshige S., 1992, MNRAS, 258, 189
Rybicki G.B., Lightman A.P., 1979, Radiative processes in astrophysics. Wiley & Sons, New York
Shakura N.I., Sunyaev R.A., 1973, A&A, 24, 337
Socrates A., Davis S.W., Blaes O., 2004, ApJ, 601, 405
Soria R., Puchnarewicz E.M., 2002, MNRAS, 329, 456
Szuszkiewicz E., Malkan M.A., Abramowicz M.A., 1996, ApJ, 458, 474
Wang J.-M., Zhou Y.-Y., 1999, ApJ, 516, 420
Wang J.-M., Szuszkiewicz E., Lu F.-J., Zhou Y.-Y., 1999, ApJ, 522, 839
Wang Q.D., 2002, MNRAS, 332, 764
Watarai K.-y., Fukue J., Takeuchi M., Mineshige S., 2000, PASJ, 52, 133
Watarai K.-y., Mizuno T., Mineshige S., 2001, ApJ, 549, L77
Watarai K.-y., Ohsuga K., Takahashi R., Fukue J., 2005, PASJ, 57, 513